Nonlinear Characteristics of the Surface Air Temperature over Canada

Aiming Wu and **William W. Hsieh**
Department of Earth and Ocean Sciences, University of British Columbia
Vancouver, B.C., V6T 1Z4, Canada
Email: awu@eos.ubc.ca, Tel: (604) 822-3932, Fax: (604) 822-6091

Amir Shabbar
Climate Research Branch, Meteorological Service of Canada
Downsview, Ontario, M3H 5T4, Canada

Submitted to J. Geophys. Res. (Atmos.) June 2001

Accepted May 2002

Abstract

Nonlinear characteristics of the Canadian surface air temperature (SAT) were investigated by applying a neural-network-based nonlinear principal component analysis (NLPCA) method to the SAT anomaly data for individual seasons. The SAT data were separated into 3 subsets: data for 1900-49 and 1900-95 over southern Canada (south of 60°N), called *S0049* and *S0095*, respectively, and data for 1950-95 over the entire country, called *C5095*. The NLPCA was computed for the three datasets separately. The leading NLPCA modes from *C5095* and *S0095* show similar results: the nonlinearity is strong in winter (DJF) and fall (SON), but is much weaker in spring (MAM) and summer (JJA), manifesting the seasonal dependence of the nonlinearity in the Canadian SAT. No significant nonlinearity is detected from dataset *S0049*, even for the winter and fall seasons, indicating interdecadal dependence of the nonlinearity. The leading NLPCA mode combines the effects of Pacific-North America (PNA) pattern and Norther Atlantic Oscillation (NAO) on the Canadian winter SAT. A possible reason for the existence of nonlinearity in the winter SAT only after 1950 is that the NAO manifested its strong negative phase from the 1950s to the early 1970s.

1 Introduction

North America is an area of interest for climate studies related to the El Niño-Southern Oscillation (ENSO) phenomenon [Horel and Wallace, 1981; Wallace and Gutzler, 1981; Trenberth *et al.*, 1998]. The traditional view is that the climate variations associated with El Niño-Southern Oscillation (ENSO) are linear, with anomalies during the El Niño phase being the reverse of those during the La Niña phase [*e.g.* Ropelewski and Halpert, 1989; Bunkers *et al.*, 1996]. However, recent evidence shows that the atmospheric responses to warm and cold events were not exactly opposite. Richman and Montroy [1996] examined the composite January temperature and precipitation patterns over the United States and parts of Canada associated with El Niño and La Niña events. Their results suggest that El Niño and La Niña have their own unique characteristics in terms of temperature and precipitation, so the responses are not linear. Asymmetric spatial patterns of the Canadian surface air temperature and precipitation associated with the Southern Oscillation (SO) were detected by Shabbar and Khandekar [1996] and Shabbar *et al.* [1997]. Further evidences of nonlinear response of North America climate to ENSO were provided by Hoerling *et al.* [1997], who suggested that the mid-latitude atmospheric response to the different phases of the SO is inherently nonlinear, due to differences in the locations of the intense tropical Pacific SST-induced deep convection between El Niño and La Niña events. From the phase shift in the mid-latitude geopotential height anomalies during the opposite phases of the SO, they concluded that mid-latitude temperature and precipitation patterns should also have nonlinear relations with the SO. The robustness of nonlinear climate response to ENSO's extreme phases was then confirmed by four GCMs [Hoerling *et al.*, 2001]. A nonlinear identification of the atmospheric response to ENSO was also addressed by Hannachi [2001] using state-of-the-art general circulation models.

Describing the nonlinear behaviour in the mid-latitude climate and its nonlinear relations to ENSO is a great challenge. Standard multivariate statistical techniques such as principal component analysis (PCA, also known as EOF analysis) and canonical correlation analysis (CCA) are linear methods. Composite analysis does not assume linearity, but is restricted to the analysis of differences between specific phases of the SO or equatorial sea surface temperature (SST) indices. Are there general methods which can describe the nonlinearity of the mid-latitude climate variability and its nonlinear relations to ENSO? Recently, neural networks (NN) [Hsieh and Tang, 1998] have been used for nonlinear PCA (NLPCA) [Kramer, 1991] and nonlinear CCA (NLCCA) [Hsieh, 2000]. The tropical Pacific SST and sea level pressure fields have recently been analyzed by the NLPCA [Monahan 2001] and by NLCCA [Hsieh, 2001a], where SST was found to exhibit considerable nonlinearity, while the sea level pressure was found to be less nonlinear. Also NLPCA was applied to the analysis of the winter Northern hemisphere atmospheric variability [Monahan *et al.*, 2000]. Hsieh [2001b] pointed out that NLPCA unifies the PCA and rotated PCA approaches.

In this paper, the NLPCA model of Hsieh [2001b] will be applied to study the surface air temperature (SAT) variability over Canada. The motivation of this paper is to examine the nonlinear characteristics of the Canadian SAT using NLPCA, before we build our prediction models using NLCCA to link the SAT and the tropical Pacific SST. The paper is organized as follows: The data are briefly introduced in Section 2. The leading NLPCA modes for the Canadian SAT data for 1950-95 over the entire country, and for 1900-95 and 1900-49 over southern Canada (south of 60°N) are presented in Section 3. Some possible dynamics related to the NLPCA mode of Canadian winter SAT are discussed in Section 4. A Summary with concluding remarks is given in Section 4. Details of the NLPCA model are described in the Appendix.

2 Data

The basic data we used in this study is the gridded monthly mean surface air temperatures (SAT) interpolated from the station observations for the period of January, 1900 to December, 1995 [Vincent and Gullet, 1999]. With this data (up to 1998), Zhang *et al.* [2000] analyzed the trend of Canadian SAT in the 20th century. Following Zhang *et al.* [2000], we separated the data into three subsets: data for 1900-49 and for 1900-95 over southern Canada (south of 60°N), called *S0049* and *S0095*, respectively, and data for 1950-95 over whole Canada, called *C5095*. There are two reasons for doing so: (a) the limited data availability in northern Canada prior to 1950; (b) a check on the significance of the NLPCA results. If the NLPCA results are reproducible from different datasets, then the nonlinearity can be regarded as robust rather than sampling dependent. The SAT data have an approximately linear trend (see Zhang *et al.*, 2000, Fig. 3), so linear-detrending was performed first. Monthly SAT anomalies were calculated by removing the climatological monthly mean based on the whole period of each dataset. The anomaly data were then smoothed with a 3-month running mean. The SAT anomalies were separated into 4 seasons: SAT anomalies in December, January, and February (DJF) were used to form a dataset for the winter season, March, April and May (MAM) for the spring, June, July and August (JJA) for the summer, and September, October and November (SON) for the fall.

The 500-mb geopotential height came from the National Centers for Environmental Prediction's (NCEP) reanalysis datasets for the period from January 1948 to December 1995 with a 2.5° grid over a global domain [Kalnay *et al.*, 1996]. The monthly SST was from the reconstructed global historical SST datasets by Smith *et al.* [1996] for the period 1950-2000 with a resolution of 2° by 2° over global oceans. Anomalies for the 500-mb height and SST fields are calculated with respect to climatological monthly means for 1950-95. Linear detrending and 3-month running mean were then performed on both datasets.

The winter (December through March) index of the North Atlantic Oscillation (NAO), defined as the difference of normalized sea level pressure (SLP) between Lisbon, Portugal and Stykkisholmur/Reykjavik, Iceland since 1864 to 2001, was provided by Dr. Jim Hurrel of the National Center for Atmospheric Research (NCAR). The SLP anomalies at each station were normalized by dividing the seasonal mean pressure by the long-term (1864-1983) standard deviation. The NAO index used in this paper is an update of the time series published in Hurrel [1995].

3 The leading NLPCA mode of Canadian SAT

3.1 *C5095*

Prior to NLPCA, traditional PCA (or EOF analysis) was performed on the SAT anomalies of each season. Variance contributions from the 4 leading modes are listed in Table 1 and the spatial patterns for the 3 leading modes are shown in Fig. 1. We can see that spatial patterns of individual seasons are very similar to each other, except that mode 2 and mode 3 of the spring data are interchanged. The first mode is uniform in sign (except the west coast for the summer) by indicating either warm or cold conditions over the whole domain, while the second mode displays a southwest-northeast contrast. For each season, the first mode can always explain 40-50% of the total variance, and the second mode about 20%. The 4 leading modes explain altogether about 80% of the total variance. The 4 leading principal components (PCs) (i.e. EOF time coefficients) are thus used as the inputs to the NLPCA model (Fig. 2).

The first NLPCA modes of SAT anomalies for four seasons are shown in Fig. 3. For convenience, 3-dimensional figures are used, where we can see not only the NLPCA curve in the PC_1-PC_2-PC_3 3-D space but also its projections on PC_1-PC_2, PC_1-PC_3 and PC_2-PC_3 planes. In winter (Fig. 3a), we can find a notable curve in the PC_1-PC_2 plane, which indicates considerable nonlinearity, relative to the PCA (straight line). 53.7% of the variance of the original data is explained by the NLPCA mode 1, versus 44.6% by the PCA mode 1. The MSE (mean square error) for the NLPCA mode is much smaller than that for the PCA mode with a ratio of 0.865. Here MSE is the mean square of the distance between a data point and its projection onto the NLPCA (or PCA) mode, i.e. the unexplained variance. The MSE ratio can be considered an indicator of the nonlinearity— as a ratio of 1 or close to 1 means the NLPCA is essentially linear, while a smaller MSE ratio means stronger nonlinearity.

Fig. 3b and 3c show relatively weak nonlinearity in the spring and summer data, with

MSE ratios of 0.965 and 0.977, respectively, and with slightly higher variance contributions (Table 2) relative to their PCA mode 1 counterparts (Table 1). The nonlinearity is then enhanced during the fall, as manifested in the increased curvature (Fig. 3d). The NLPCA mode 1 for the fall data accounts for 51.8% of the total variance, versus 40.1% by the PCA mode 1. The MSE ratio is 0.833, indicating a little higher nonlinearity than during winter.

Unlike a PCA mode, which produces a fixed spatial pattern (the EOF), the NLPCA mode does not give a single characteristic spatial pattern. For a specific value of the NLPC u (see Appendix), we can use the NN to map u in the bottleneck neuron onto $\mathbf{x}'$ in the output layer (Fig. 2) using Eqs 5,6 (in Appendix). Note that u can be regarded as a simple curvilinear coordinate system on the NLPCA curve, and therefore each value of u corresponds to a pattern within the first 4 PCs. Fig. 4 shows the SAT anomaly patterns corresponding to minimum u and maximum u. We can see that the spatial patterns on opposite extremes of u are now asymmetric, i.e. no longer mirror images. The asymmetry is enhanced as the nonlinearity increases. The spatial patterns associated with minimum u and maximum u are basically symmetric for the summer (Fig. 4e,f), and slightly more asymmetric for the spring, with the warm center shifted southward relative to the cooling center in Fig. 4c,d. The spatial asymmetry gets enhanced in the fall and winter. For the fall, the minimum and maximum u patterns have respectively negative and positive anomalies basically covering the whole domain. But the cold pattern is centered over the northeast (Fig. 4g), and the warm pattern is centered towards the west (Fig. 4h). The spatial patterns for opposite values of u are also quite asymmetric during the winter. At maximum u, there are positive anomalies over all of Canada (Fig. 4b), similar to the EOF_1

(Fig. 1a), with the warm center over western Canada. At minimum u, there are negative anomalies to the southwest and positive anomalies to the northeast, similar to the EOF_2 (Fig. 1b). It is not surprising because the NLPCA mode 1 combines PC1 and PC2 (Fig. 3a).

It is worth noting that the winter SAT anomaly pattern associated with maximum u (Fig. 4b) is similar to the composite results during El Niño years [Hoerling *et al.*, 1997, 2001], while the SAT anomaly pattern associated with minimum u (Fig. 4a) is different from their composite results during La Niña years. Therefore, the NLPCA mode reveals the possible effects from more than ENSO on the Canadian SAT. This will be further discussed later in this paper.

3.2 *S0095*

Similarly, traditional PCA was performed on the SAT anomalies of *S0095* for each season to compress the data and the first three EOFs are shown in Fig. 5. The EOF1 and EOF2 are roughly consistent with those of *C5095*, while the EOF3 patterns are different from those shown in Fig. 1. The variance contributions for the four leading modes are listed in Table 1. The first 4 PCs are used as the inputs to the NLPCA.

The first NLPCA modes of SAT for four seasons are shown in Fig. 6, where we can see similar results as extracted from *C5095* although the NLPC curves are not exactly the same. The strongest nonlinearity occurs in winter with a MSE ratio of 0.879, followed by the fall with a MSE ratio of 0.908. The NLPCA modes explain 63.4% and 60.8% of the total variance of the winter and fall SAT anomalies, respectively, versus 58.2% and 55.4%

by the PCA modes. Fig. 6b and 6c show rather weak nonlinearity in the spring and summer data (see also Table 2).

In the spatial patterns (Fig. 7), for the spring (Fig. 7c,d) and summer (Fig. 7e,f), the SAT anomalies on opposite extremes of the NLPC u are basically similar except for a sign change, resembling their EOF1 patterns (Fig. 5d and 5g). More asymmetry can be seen in the winter (Fig. 7a,b) and fall (Fig. 7g,h), and the spatial patterns are in reasonably good agreement with those shown in Fig. 4a,b and Fig. 4g,h, respectively. Although *C5095* and *S0095* are partially overlapping (not completely independent), the similarity of the NLPCA results from two datasets suggests the significance of the seasonal dependence of the nonlinearity of the Canadian SAT, at least for the data after the 1950s.

3.3 *S0049*

S0049, which is completely independent of *C5095*, is considered in this section. Spatial patterns of the first 3 PCA modes, shown in Fig. 8, are well consistent with those extracted from *S0095* (Fig. 5, except for the opposite sign in EOF2 for the winter, spring and summer). Detail information for the PCA modes are listed in Table 1. The first 4 PCs serve as the inputs to the NLPCA.

The first NLPCA modes of SAT anomalies for four seasons are shown in Fig. 9. If disregarding the few outlier points (*e.g.* in Fig. 9d), no notable nonlinearity can be seen in any of the four seasons. Table 2 indicated that the MSE ratios are all above 0.95 and the explained variance percentage differences between nonlinear and linear modes are also small (not over 2.0%), implying rather weak nonlinearity. The spatial anomaly patterns associated with minimum u and maximum u are generally symmetric for all four seasons (figures not shown), confirming the weak nonlinearity again.

Since *S0095* exhibits considerable nonlinearity in winter and fall, while *S0049* does not show apparent nonlinearity for all four seasons, nonlinearity for the winter and fall exists mainly in the data after 1950s, suggesting interdecadal dependence in the nonlinearity of the Canadian SAT.

4 Dynamics related to Canadian SAT NLPCA mode

4.1 Winter 500-mb height

As the strong nonlinearity tends to occur in winter, we will examine the winter season more closely. Regressions of a winter SAT EOF PC onto the global 500-mb height anomalies (1950-95) reveal the spatial patterns of the 500-mb heights co-varying with the PC, which was standardized first. The 1st winter SAT PC regressed onto the simultaneous 500-mb height anomalies revealed a Pacific-North American (PNA) pattern, where there is generally positive height anomalies over Canada, and negative height anomalies over the mid-latitude North Pacific and the southeastern United States when the PC is positive (Fig. 10a), corresponding to warming over whole Canada (Fig. 4b). The 2nd SAT PC regressed onto the winter 500-mb height anomalies gave a North Atlantic Oscillation (NAO) pattern, with a large negative anomaly centered over southwestern Greenland and northeastern Canada, and a large positive anomaly centered over western Europe and a positive anomaly over the west coast of Canada when the PC is positive (Fig. 10b), corresponding to warm western

Canada and cool eastern Canada (Fig. 4a with signs reversed). Since major nonlinearity occurs between PC_1-PC_2 (Fig. 3a and 6a), the leading NLPCA mode thus combines the effects of PNA and NAO on the Canadian winter SAT, suggesting that the effects of PNA and NAO on Canada may not be totally independent. It appears that the SAT PC_2 tends to take on negative values when PC_1 takes on significant negative values (Fig. 3a), i.e. negative NAO effects, a warm eastern Canada – cool western Canada (Fig. 1b with signs reversed), tends to concur with negative PNA effects (cool Canada) (Fig. 1a with signs reversed).

4.2 The global SST

Similar regressions of a winter SAT PC onto the global SST anomalies were performed. The regressions of the 1st winter SAT PC onto SST anomalies yielded a spatial pattern resembling the Pacific Decadal Oscillation (PDO, Trenberth and Hurrell, 1994), i.e. when the PC is positive (corresponding to warm Canada, Fig. 1a), there is cool SST over the central-western mid-latitude North Pacific and warm waters off the west coast of North America (Fig. 10c), which is consistent with the ocean's response to the PNA pattern in the atmosphere. The 3rd SAT PC regressed on the SST anomalies manifested a pattern somewhat similar to ENSO, i.e. warm SST in the eastern-central equatorial Pacific (Fig. 10d) when the 3rd PC is positive, corresponding to warm southern Canada and cool northern Canada (Fig. 1c).

4.3 Nonlinearity and the NAO

We take a closer look at the NLPCA mode for *S0095* and *S0049* in Fig. 11 (only projections on the PC_1-PC_2 plane are shown). *S0095* and its NLPCA mode are shown by the symbols of plus and overlapping circles, while *S0049* and its NLPCA mode, by scattered dots and squares, respectively. For comparison, the signs of PC_2, also the PC_2 at the output layer of NLPCA model of *S0049* are reversed since the EOF2 of *S0049* (Fig. 8b) is opposite in sign to the EOF2 of *S0095* (Fig. 5b). We can see the symbols of '+' and '.' at the same time (1900-49) are close but not exactly overlapping, as the EOFs for two datasets are similar but not identical (Fig. 5a-c and Fig. 8a-c). Regarding the NLPCA modes, if we ignore the data points of *S0095* in the big circle (Fig. 11), the two NLPC curves could be very similar, i.e. it is these points that brings the nonlinearity to *S0095*. These data points are to be found in the winters of 1916, 1933, 1937, 1951, 1955, 1956, 1965, 1966, 1968, 1969, 1977 and 1982. These years have negative NAO index values (Fig. 12), except for 1933, 1937 and 1982, and most of them are within the period of 1951-77. Actually, after a 7-year running mean, the NAO index (thick line in Fig. 12) is basically positive from 1900 to 1930, normal in the 1930s and 1940s and negative from 1952 to the early 1970s and then turns to be positive after the mid 1970s, reaching its positive extreme in the early 1990s. It is possible that the existence of the nonlinearity in the Canadian winter SAT only after the 1950s is due to the strong negative phase of the NAO occurring from 1950s to the early 1970s. The negative NAO pattern (Fig. 10b with signs reversed) and the resulting SAT patterns shown in Fig. 4a and 7a are more likely to occur during the negative phase of the NAO.

To check that the downward curve in *S0095* (Fig. 11) is not due to the outliers from a single year, we removed the data from winter 1969 (which contributed the two points with the most negative PC_2 values) and re-computed the NLPCA solution, which again yielded the downward curve found in Fig. 11.

5 Concluding remarks

NLPCA was performed on three subsets of the Canadian seasonal surface air temperatures (SAT): 1900-49 and 1900-95 over southern Canada (south of 60°N), and 1950-95 over the entire country— with the three datsets named *S0049*, *S0095* and *C5095*, respectively. The SAT anomalies were found to be generally linear during 1900-49 for all seasons in *S0049*. However, after 1950, the SAT anomalies showed considerable nonlinearity in winter (DJF) and fall (SON) (but much weaker nonlinearity in spring and summer), indicating interdecadal and seasonal dependence in the nonlinearity of the Canadian SAT. During winter, the leading NLPCA model reveals asymmetric SAT anomaly patterns– at one extreme of the NLPCA mode, there are negative NAO effects with a warm eastern Canada-cool western Canada pattern (Fig. 4a), and at the other extreme, positive PNA effects with warming over all of Canada (Fig. 4b). The negative NAO effects also tend to concur with negative PNA effects, suggesting that the PNA and NAO effects on Canadian SAT may not be independent, and the NLPCA has been successful in combining the effects of the two.

The absence of notable nonlinearity in the SAT anomalies during 1900-49 was puzzling. Since nonlinearity was found in the data during 1900-95 (*S0095*), this implied nonlinearity of considerable strength in the data after 1950. In fact, the NLPCA mode 1 results from dataset *S0095* agreed well with those from dataset *C5095*, confirming the robustness of the nonlinearity found in the SAT anomalies in the later period of 1950-95. Still, there is a concern that the nonlinearity detected in the 1950-95 period was due to sampling, as nonlinearity was not detected in the 1900-49 period. Indeed with short climate records, this possibility cannot be ruled out. However, in the last section, our test with the outlier winter 1969 data removed from the NLPCA calculation at least eliminated the possibility that the detected nonlinearity arose from a single outlier year. Furthermore, as negative NAO effects contributed to the nonlinearity in the winter SAT, and strong negative NAO occurred during the 1950s to the early 1970s but not during the 1900-49 period, this could be a reason for the absence of significant nonlinearity in the winter SAT data before 1950.

The temporal relationship between the NAO and ENSO was investigated by Huang *et al.* [1998] using a multiresolution cross-spectral technique. Their results show significant coherence between NAO and Niño3 SST in about 70% of the warm events from 1900 to 1995, i.e., the strong El Niño events concur with the positive phase of the NAO. During relatively weak Niño3 SST anomalies, they found a teleconnection pattern which shows a strong negative phase of the NAO and a pattern resembling a weak eastward-shifted negative PNA pattern. Interestingly, their results generally corroborate the findings in this paper.

Appendix: The NLPCA method

A variable $\mathbf{x}$, which consists of l spatial stations and n observations in time, can be expressed in the form $\mathbf{x}(t) = [x_1, \ldots, x_l]$, where $x_i, (i = 1, 2, \ldots, l)$, is a time series of length n. PCA is to find a scalar variable u and an associated vector $\mathbf{a}$, with

$$u(t) = \mathbf{a} \cdot \mathbf{x}(t)\,, \tag{1}$$

so that

$$\langle \|\mathbf{x}(t) - \mathbf{a}u(t)\|^2 \rangle \;\text{ is minimized,} \tag{2}$$

where $\langle \cdots \rangle$ denotes a sample or time mean. Here u, called the first principal component (PC), is a time series resulting from a linear combination of the original variables x_i, while $\mathbf{a}$, the first eigenvector of the data covariance matrix, (also called an empirical orthogonal function, EOF), often describes a spatial pattern. From the residual, $\mathbf{x}-\mathbf{a}u$, the second PCA mode can similarly be extracted, and so on for the higher modes. In practice, the common algorithms for PCA extract all modes simultaneously by calculating the eigenvalues and eigenvectors of the data corviance matrix.

The fundamental difference between NLPCA and PCA is that NLPCA allows a non-linear continuous mapping from $\mathbf{x}$ to u whereas PCA only allows a linear mapping. To perform NLPCA, the NN in Fig. 2 contains 3 'hidden' layers of variables (or 'neurons') between the input and output layers, called the encoding layer, bottleneck, and decoding layer, respectively.

Following Hsieh (2001b), four transfer functions f_1, f_2, f_3, f_4 are used to map from the input layer to the output layer ($\mathbf{x} \longrightarrow \mathbf{h}^{(x)} \longrightarrow u \longrightarrow \mathbf{h}^{(u)} \longrightarrow \mathbf{x}'$):

$$h_k^{(x)} = f_1((\mathbf{W}^{(x)}\mathbf{x} + \mathbf{b}^{(x)})_k)\,, \tag{3}$$

$$u = f_2(\mathbf{w}^{(x)} \cdot \mathbf{h}^{(x)} + \overline{b}^{(x)})\,, \tag{4}$$

$$h_k^{(u)} = f_3((\mathbf{w}^{(u)}u + \mathbf{b}^{(u)})_k)\,, \tag{5}$$

$$x_i' = f_4((\mathbf{W}^{(u)}\mathbf{h}^{(u)} + \overline{\mathbf{b}}^{(u)})_i)\,, \tag{6}$$

where the capital bold font is reserved for matrices and the small bold font for vectors, $\mathbf{x}$ is the input column vector of length l, $\mathbf{h}^{(x)}$, a column vector of length m (m is the number of the hidden neurons in the encoding layer), $\mathbf{W}^{(x)}$ is an $m \times l$ weight matrix, $\mathbf{b}^{x}$, a column vector of length m containing the bias parameters, and $k \in [1, m]$. The bottleneck layer contains a single neuron, which represents the nonlinear principal component u. The decoding layer contain the same number of neurons m as the encoding layer, and the output layer is also a column vector of length l.

The transfer functions f_1 and f_3 are generally nonlinear (here taken to be the hyperbolic tangent function), while f_2 and f_4 are taken to be the identity function. If the transfer functions f_1 and f_3 are also replaced by a linear function, NLPCA essentially reduces to PCA.

The cost function $J = \langle \|\mathbf{x} - \mathbf{x}'\|^2 \rangle$ is minimized by finding the optimal values of $\mathbf{W}^{(x)}$, $\mathbf{b}^{(x)}$, $\mathbf{w}^{(x)}$, $\overline{b}^{(x)}$, $\mathbf{w}^{(u)}$, $\mathbf{b}^{(u)}$, $\mathbf{W}^{(u)}$ and $\overline{\mathbf{b}}^{(u)}$. The MSE (mean square error) between the NN output $\mathbf{x}'$ and the original data $\mathbf{x}$ is thus minimized.

Generally, we can impose the constraint $\langle u \rangle = 0$, hence

$$\overline{b}^{(x)} = -\langle \mathbf{w}^{(x)} \cdot \mathbf{h}^{(x)} \rangle\,. \tag{7}$$

The total number of free (weight and bias) parameters to be determined is then $2lm + 4m + l$. Furthermore, we adopt the normalization condition that $\langle u^2 \rangle = 1$. This condition is approximately satisfied by modifying the cost function to

$$J = \langle \|\mathbf{x} - \mathbf{x}'\|^2 \rangle + (\langle u^2 \rangle - 1)^2 \,. \tag{8}$$

The most serious problem with NLPCA is the presence of local minima in the cost function. As a result, optimizations started from different initial parameters often converge to different minima, rendering the method unstable. This problem can be effectively avoided by adding a weight penalty term into the cost function (Hsieh, 2001b).

$$J = \langle \|\mathbf{x} - \mathbf{x}'\|^2 \rangle + (\langle u^2 \rangle - 1)^2 + p \sum_{ki} (W_{ki}^{(x)})^2 \,, \tag{9}$$

where p is the weight penalty parameter. With p, the concavity of the cost function is increased, pushing the weights $\mathbf{W}^{(x)}$ to be smaller in magnitude, thereby yielding smoother and less nonlinear solutions than when p is small or zero. With a large enough p, the danger of overfitting is greatly reduced, hence the optimization can proceed until convergence to the global minimum.

The nonlinear optimization was carried out by the MATLAB function 'fminu', a quasi-Newton algorithm. Despite of the weight penalty, there is still no guarantee that the optimization algorithm reaches the global minimum. Hence an ensemble of 60 NNs with random initial weights and bias parameters was run. Also, 20% of the data was randomly selected as test data and withheld from the training of the NNs. Runs where the MSE was larger for the test dataset than for the training dataset were rejected to avoid overfitted solutions. Then the NN with the smallest MSE was selected as the solution. The NLPCA was run repeatedly with $m = 2$ and 3, and 30 values of p ranging from 0 to 0.18, then the solution with the smallest MSE was chosen as the desired solution.

Acknowledgements

This work was supported by a strategic grant to Hsieh and Shabbar from the Natural Sciences and Engineering Research Council of Canada, and a contract to Hsieh from the Meteorological Services of Canada. We thank Francis Zwiers for helpful comments.

References

Bunkers, M.J., J.R. Miller and A.T. DeGaetano, An examination of the El Niño or La Niña related precipitation and temperature anomalies across the northern plains, *J. Climate, 9,* 147-160, 1996.

Hannachi, A., Toward a nonlinear identification of the atmospheric response to ENSO, *J. Climate, 14,* 2138-2149, 2001.

Hoerling, M.P., A. Kumar, and M. Zhong, El Niño, La Niña and the nonlinearity of their teleconnections, *J. Climate, 10,* 1769-1786, 1997.

Hoerling, M.P., A. Kumar, and T. Xu, Robustness of the nonlinear climate responses to ENSO's extreme phases, *J. Climate, 14,* 1277-1293, 2001.

Horel, J,D., and J.M. Wallace, Planetary scale atmospheric phenomena associated with the Southern Oscillation. *Mon. Wea. Rev., 109,* 813-929, 1981.

Hsieh, W.W. and B. Tang, Applying neural network models to prediction and data analysis in meteorology and oceanography, *Bull. Amer. Meteor. Soc., 79,* 1855-1870, 1998.

Hsieh, W.W., Nonlinear canonical correlation analysis by neural networks, *Neural Networks, 13,* 1095-1105, 2000.

Hsieh, W.W., Nonlinear canonical correlation analysis of the tropical Pacific climate variability using a neural network approach, *J. Climate*, *14,* 2528-2539, 2001a.

Hsieh, W.W., Nonlinear principal component analysis by neural networks, *Tellus, 53A,* 599-615, 2001b.

Huang, J., K. Higuchi and A. Shabbar, The relationship between the North Atlantic Oscillation and the El Niño-Southern Oscillation, *Geophy. Res. Lett., 25,* 2707-2710, 1998.

Hurrel, J.W., Decadal trends in the North Atlantic Oscillation: regional temperatures and precipitation networks, *Sciences, 269,* 676-679, 1995.

Kalnay, E., M. Kanamitsu, R. Kisler, W. Collins, D. Deaven, L. Gandin, M. Iredell, S. Sasha, G. White, J. Woolen, Y. Zhu, M. Chelliah, W. Ebisuzaki, W. Higgins, J. Janowiak, K.C. Mo, C. Ropelewski, J. Wang, A. Leetmaa, R. Reynolds, R. Jenne, and Dennis Joseph, the NCEP/NCAR 40-year reanalysis project. *Bull. Amer. Meteor. Soc., 77,* 437-471, 1996.

Kramer, M.A., Nonlinear principal component analysis using autoassociative neural networks, *AIChE Journal, 37,* 233-243, 1991.

Monahan, A.H., J.C. Fyfe and G.M. Flato, A regime view of Northern Hemisphere atmospheric variability and change under global warming, *Geophy. Res. Lett., 27,* 1139-1142, 2000.

Monahan, A.H., Nonlinear principal component analysis, Tropical Indo-Pacific sea surface temperature and sea level pressure, *J. Climate, 14,* 219-233, 2001.

Richman, M.B. and D.L. Montroy, Nonlinearities in the signal between El Niño/La Niña events and North American precipitation and temperature, Preprints, *13th Conf. on Probability and Statistics in the Atmospheric Sciences,*, San Francisco, CA, Amer. Meteor. So., 90-97, 1996.

Ropelewski, C.F. and M.S. Halpert, Precipitation patterns associated with the high index phase of the Southern Oscillation, *J. Climate, 2,* 268-284, 1989.

Shabbar, A. and M. Khandekar, The impact of El Niño-Southern Oscillation on the temperature field over Canada, *Atmos.-Ocean, 34,* 401-416, 1996.

Shabbar, A., B. Bonsal and M. Khandekar, Canadian precipitation patterns associated with Southern Oscillation, *J. Climate, 10,* 3016-3027, 1997.

Smith, T.M., R.W. Reynolds, R.E. Livezey and D.C. Stockes, Reconstruction of historical sea surface temperatures using empirical orthogonal functions, *J. Climate, 9,* 1403-1420, 1996.

Trenberth, K.E., and J.W. Hurrell, Decadal atmosphere-ocean variations in the Pacific, *Clim. Dyn., 9,* 303-319, 1994.

Trenberth, K.E., G.W. Branstator, D. Karoly, A. Kumar, N.-C. Lau, and C. Ropelewski, Progress during TOGA in understanding and modelling global teleconnections associated with tropical sea surface temperatures. *J. Geophys. Res., 103,* 14291-14324, 1998.

Vincent, L.A., and D. Gullet, Canadian historical and homogeneous temperature datasets for climate change research, *Int. J. Clim., 19,* 1375-1388, 1999.

Wallace, J.M., and D. Gutzler, Teleconnection in the geopotential height field during the Northern Hemisphere winter. *Mon. Wea. Rev., 109,* 784-812, 1981.

Zhang X., L.A. Vincent, W.D. Hogg and A. Niitsoo, Temperature and precipitation trends in Canada during the 20th century, *Atmos.-Ocean, 38,* 395-429, 2000.

Figure Captions

Fig. 1: The first four empirical orthogonal functions (EOFs) of the seasonal surface air temperature (SAT) anomalies for 1950-95 over the entire country (*C5095*). From top to bottom, the four rows represent the winter (a-c), spring (d-f), summer (g-i) and fall (j-l), respectively. Solid curves denote positive contours, dashed curves, negative contours, and thick curves, zero contours. The contour interval is 0.02. The EOFs are normalized to unit norm.

Fig. 2: A schematic diagram of the NN model for calculating nonlinear PCA (NLPCA). There are 3 'hidden' layers of variables or 'neurons' (denoted by circles) sandwiched between the input layer $\mathbf{x}$ on the left and the output layer $\mathbf{x}'$ on the right. Next to the input layer is the encoding layer (with m hidden neurons), followed by the 'bottleneck' layer (with a single neuron u), which is then followed by the decoding layer. A nonlinear function maps from the higher dimension input space to the lower dimension bottleneck space, followed by an inverse transform mapping from the bottleneck space back to the original space represented by the outputs, which are to be as close to the inputs as possible by minimizing the cost function $J = \langle \|\mathbf{x}-\mathbf{x}'\|^{\mathbf{2}} \rangle$. Data compression is achieved by the bottleneck, with the bottleneck neuron giving u, the nonlinear principal component. The actual NLPCA used in this paper has 4 inputs (and 4 outputs), has m between 2 and 3, and adds a weight penalty term in the cost function to alleviate overfitting (see Appendix).

Fig. 3: The first NLPCA mode for the seasonal SAT anomalies of *C5095* plotted as (over-

lapping) squares in the PC_1-PC_2-PC_3 3-D space. The linear (PCA) mode is shown as a dashed line. The NLPCA mode and the PCA mode are also projected onto the PC_1-PC_2 plane, the PC_1-PC_3 plane, and the PC_2-PC_3 plane, where the project NLPCA is indicated by (overlapping) circles, and the PCA by thin solid lines, and the projected data points by scattered dots. Panels (a), (b), (c) and (d) correspond to the winter, spring, summer and fall, respectively.

Fig. 4: The SAT anomaly patterns (in °C) of the NLPCA mode 1 extracted from *C5095*, as the NLPC (i.e. u) of the first NLPCA mode takes its minimum and maximum values. Contour interval is 1°C. The 4 rows from top to bottom display the winter (a,b), spring (c,d), summer (e,f) and fall (g,h) patterns, respectively.

Fig. 5: Similar to Fig. 2, but for *S0095*. For better visualization, the values have been multiplied by 100 and drawn with contour interval of 2.

Fig. 6: Similar to Fig. 3, but for *S0095*.

Fig. 7: Similar to Fig. 4, but for *S0095*.

Fig. 8: Similar to Fig. 5, but for *S0049*.

Fig. 9: Similar to Fig. 3, but for *S0049*.

Fig. 10: The regression coefficients between the winter 1st PC (of the Canadian SAT anomalies of *C5095*) and the global simultaneous (a) 500-mb height anomalies, and (c) SST anomalies; and the regression coefficients (b) between the winter 2nd PC and the 500-mb height anomalies, and (d) between the winter 3rd PC and the SST

anomalies. The regression coefficient shown is the slope, with the PC treated as the independent variable in the regression. Contour interval is 10 in panel (a) and (b), and 0.1 in panel (c) and (d), respectively. The SAT PCs were standardized before performing regression.

Fig. 11: Projections of *S0095* and its leading NLPCA mode onto the PC_1-PC_2 plane, shown by the symbol of plus (+) and overlapping circles. Similarly, projections of *S0049* and its leading NLPCA mode, by scattered dots and overlapping squares, respectively. The big circle includes the data points which possibly contribute to nonlinearity of SAT anomalies after 1950. The straight line represents the PCA mode 1.

Fig. 12: Time series of the winter (December through March) index of the North Atlantic Oscillation (NAO), defined as the difference of normalized sea level pressure (SLP) between Lisbon and Stykkisholmur (Lisbon minus Stykkisholmur) since 1864 to 2001, shown with the hollow bars. A 7-year running mean of the NAO index is displayed by the thick line.

Table 1: Variance (in %) explained by the 4 leading EOF (PCA) modes of the seasonal SAT anomalies for 1950-95 over the entire country (*C5095*), for 1900-95 and 1900-49 over southern Canada (south of 60°N, *S0095* and *S0049*, respectively). The bottom line shows the sum of the 4 modes.

	C5095				*S0095*				*S0049*			
	DJF	MAM	JJA	SON	DJF	MAM	JJA	SON	DJF	MAM	JJA	SON
1	44.6	46.1	40.6	40.1	58.2	54.9	48.3	55.4	61.4	55.3	47.9	60.6
2	24.7	17.5	15.3	29.4	21.3	21.3	16.5	24.9	19.0	20.9	15.7	20.9
3	11.0	14.2	14.3	10.6	7.5	8.2	11.2	5.8	6.1	7.5	11.1	5.7
4	7.3	6.1	6.5	5.7	4.1	3.8	6.0	3.3	4.2	3.5	7.1	2.9
$\sum_1^4$	87.6	83.9	76.7	85.8	91.1	88.2	82.0	90.0	90.7	87.2	81.8	90.1

Table 2: Explained variance (in %) by the NLPCA mode 1 (Ev) and the ratio (R) between the MSE of the NLPCA mode 1 and that of the PCA mode 1.

	C5095				*S0095*				*S0049*			
	DJF	MAM	JJA	SON	DJF	MAM	JJA	SON	DJF	MAM	JJA	SON
Ev	53.7	48.4	41.2	51.8	63.4	55.2	48.8	60.8	62.7	56.3	48.3	61.9
R	.865	.965	.977	.833	.879	.983	.986	.908	.951	.960	.973	.958

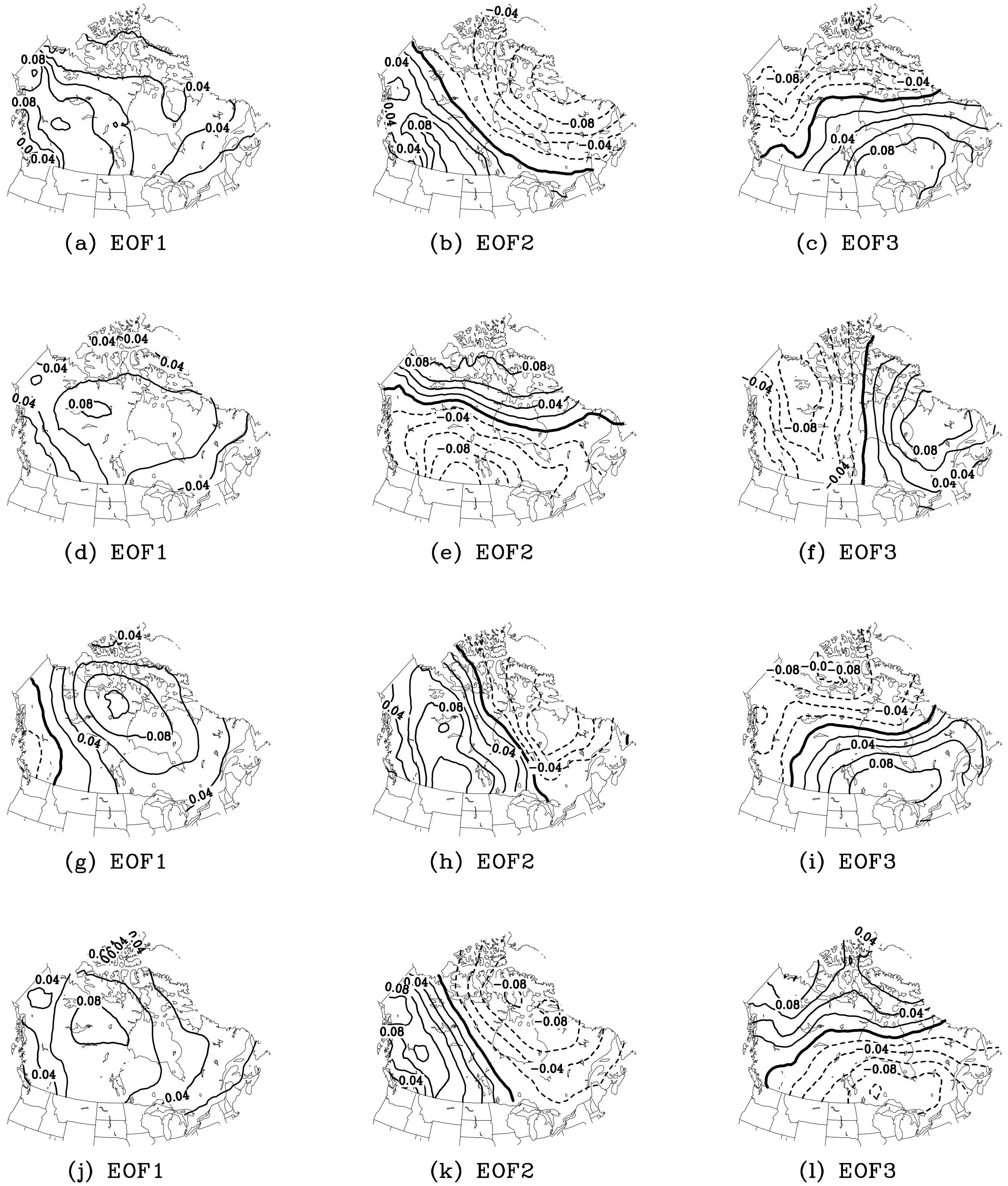

Figure 1: The first four empirical orthogonal functions (EOFs) of the seasonal surface air temperature (SAT) anomalies for 1950-95 over the entire country (*C5095*). From top to bottom, the four rows represent the winter (a-c), spring (d-f), summer (g-i) and fall (j-l), respectively. Solid curves denote positive contours, dashed curves, negative contours, and thick curves, zero contours. The contour interval is 0.02. The EOFs are normalized to unit norm.

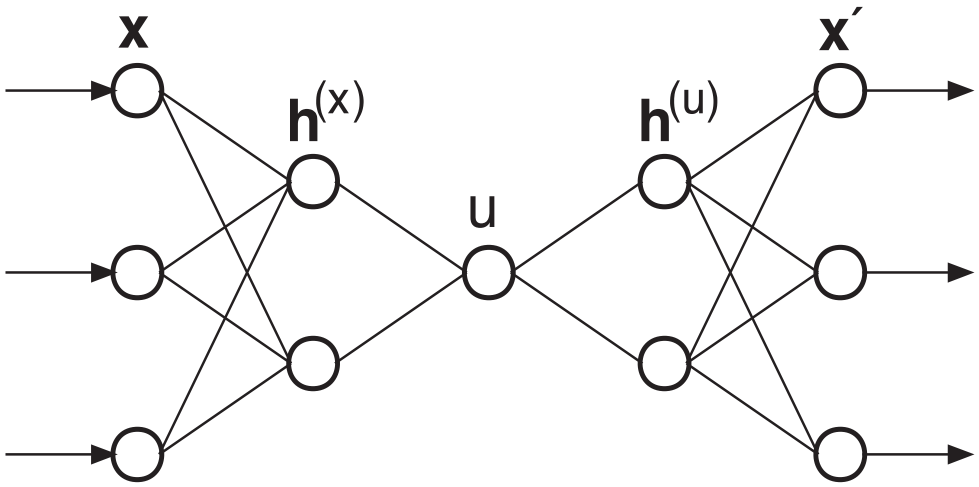

Figure 2: A schematic diagram of the NN model for calculating nonlinear PCA (NLPCA). There are 3 'hidden' layers of variables or 'neurons' (denoted by circles) sandwiched between the input layer $\mathbf{x}$ on the left and the output layer $\mathbf{x}'$ on the right. Next to the input layer is the encoding layer (with m hidden neurons), followed by the 'bottleneck' layer (with a single neuron u), which is then followed by the decoding layer. A nonlinear function maps from the higher dimension input space to the lower dimension bottleneck space, followed by an inverse transform mapping from the bottleneck space back to the original space represented by the outputs, which are to be as close to the inputs as possible by minimizing the cost function $J = \langle \|\mathbf{x} - \mathbf{x}'\|^{\mathbf{2}} \rangle$. Data compression is achieved by the bottleneck, with the bottleneck neuron giving u, the nonlinear principal component. The actual NLPCA used in this paper has 4 inputs (and 4 outputs), has m between 2 and 3, and adds a weight penalty term in the cost function to alleviate overfitting (see Appendix).

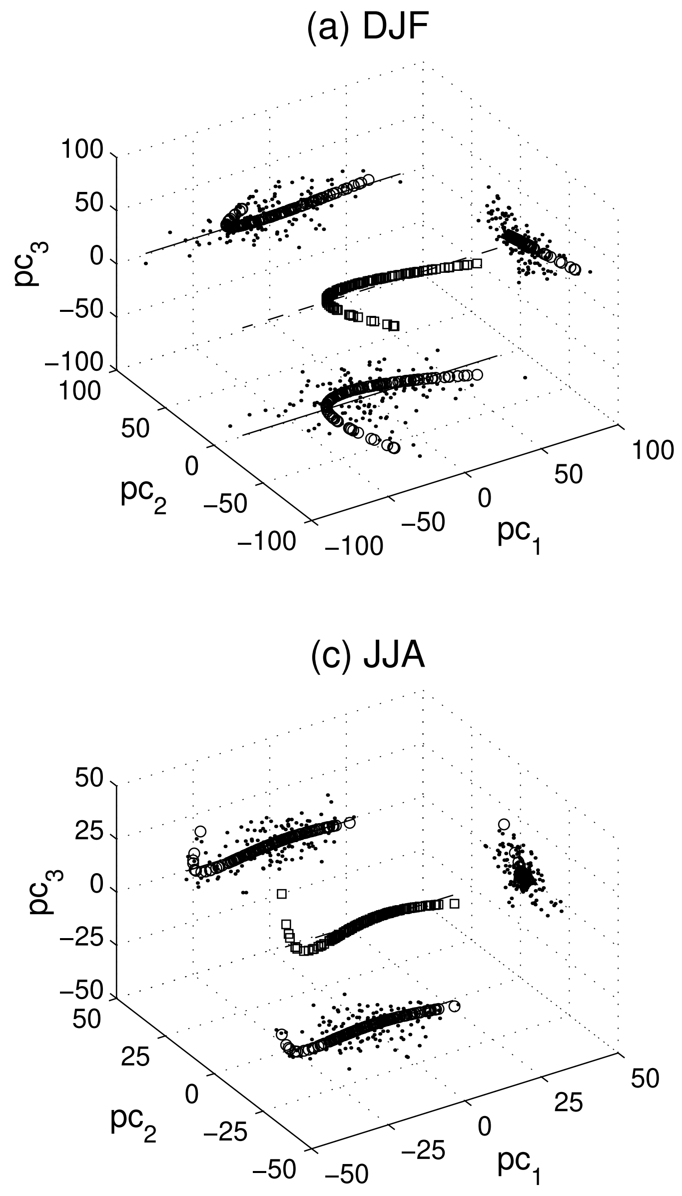

Figure 3: The first NLPCA mode for the seasonal SAT anomalies of *C5095* plotted as (overlapping) squares in the PC_1-PC_2-PC_3 3-D space. The linear (PCA) mode is shown as a dashed line. The NLPCA mode and the PCA mode are also projected onto the PC_1-PC_2 plane, the PC_1-PC_3 plane, and the PC_2-PC_3 plane, where the project NLPCA is indicated by (overlapping) circles, and the PCA by thin solid lines, and the projected data points by scattered dots. Panels (a), (b), (c) and (d) correspond to the winter, spring, summer and fall, respectively.

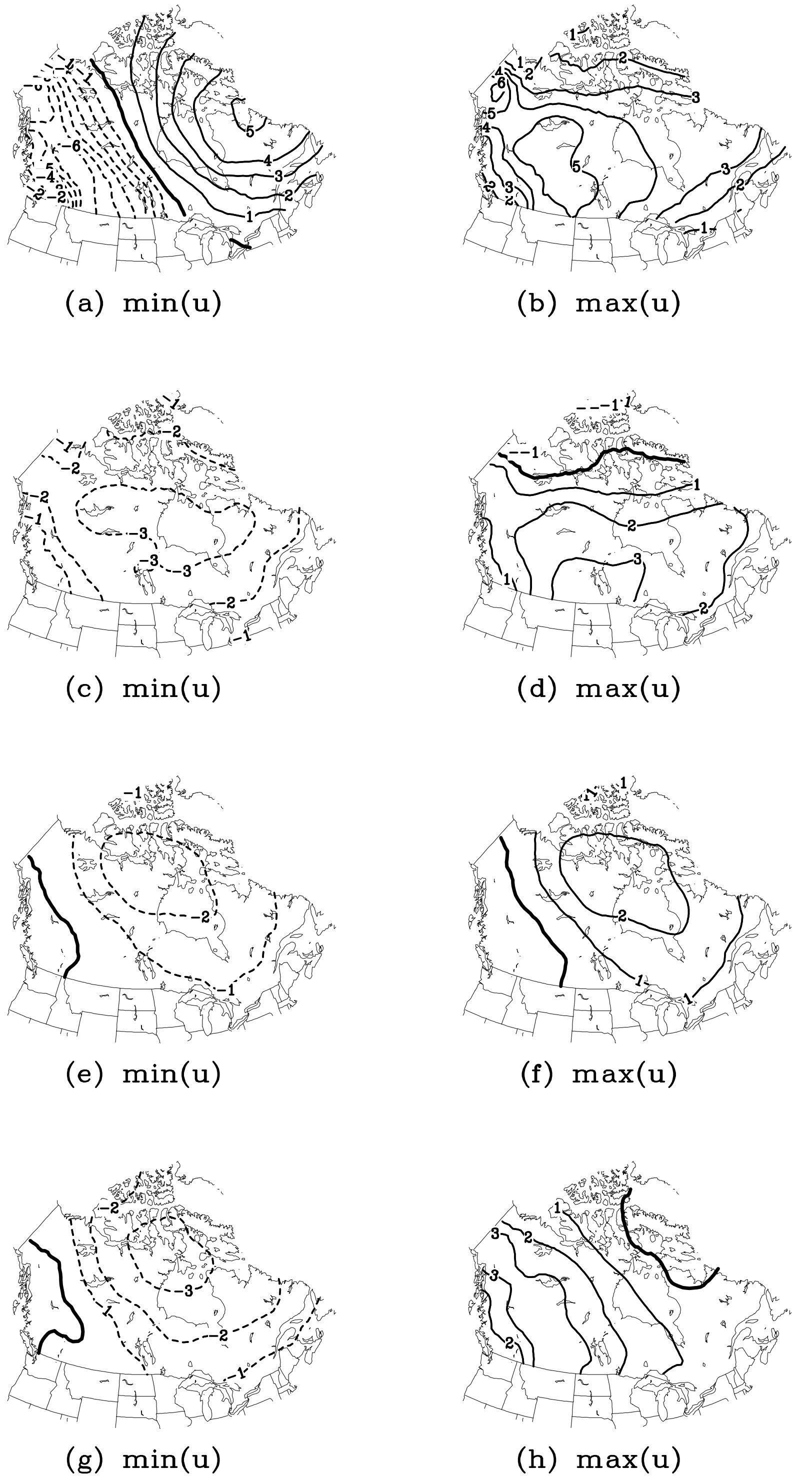

Figure 4: The SAT anomaly patterns (in °C) of the NLPCA mode 1 extracted from *C5095*, as the NLPC (i.e. u) of the first NLPCA mode takes its minimum and maximum values. Contour interval is 1°C. The 4 rows from top to bottom display the winter (a,b), spring (c,d), summer (e,f) and fall (g,h) patterns, respectively.

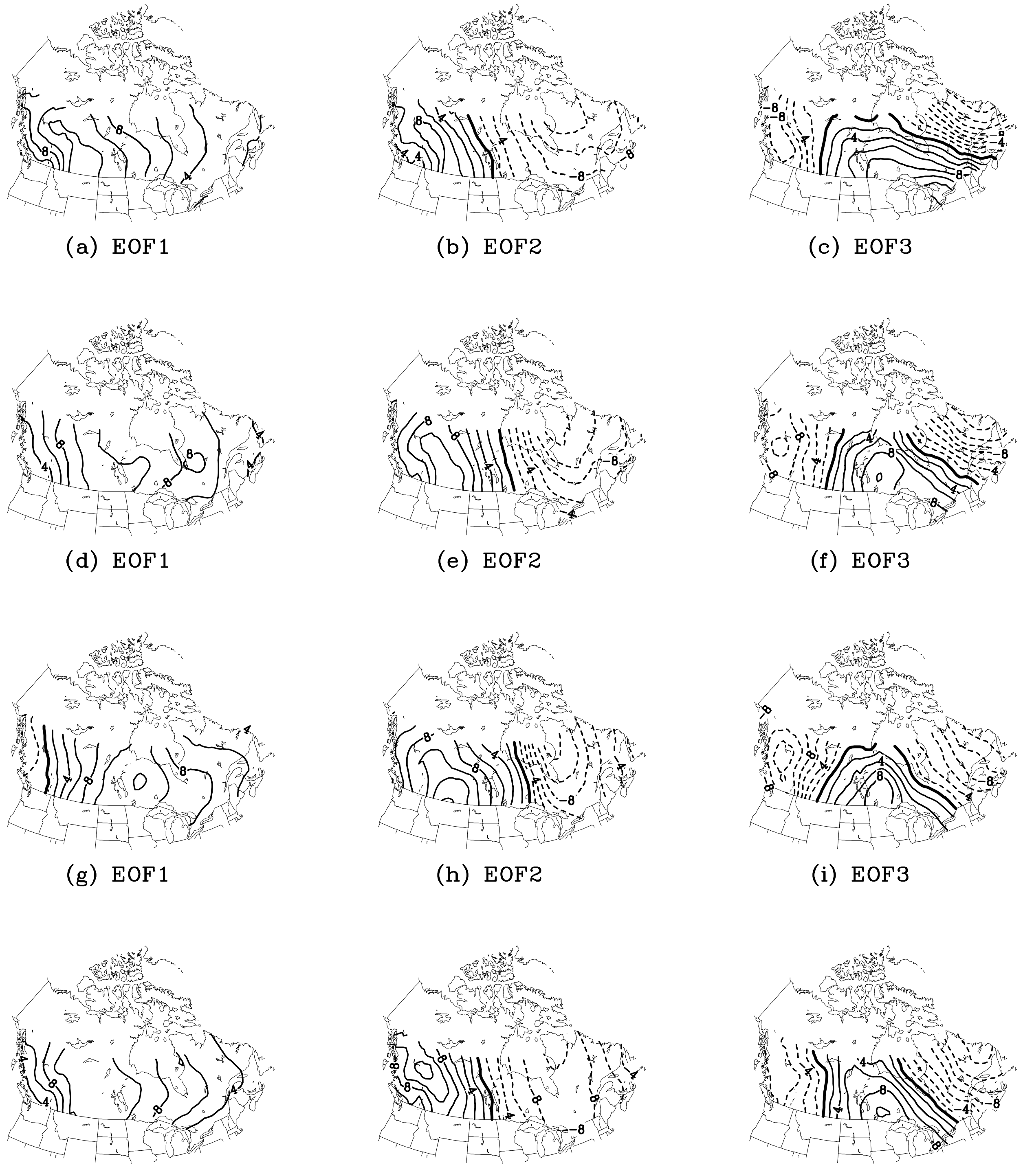

(a) EOF1 (b) EOF2 (c) EOF3

(d) EOF1 (e) EOF2 (f) EOF3

(g) EOF1 (h) EOF2 (i) EOF3

(j) EOF1 (k) EOF2 (l) EOF3

Figure 5: Similar to Fig. 2, but for *S0095.* For better visualization, the values have been multiplied by 100 and drawn with contour interval of 2.

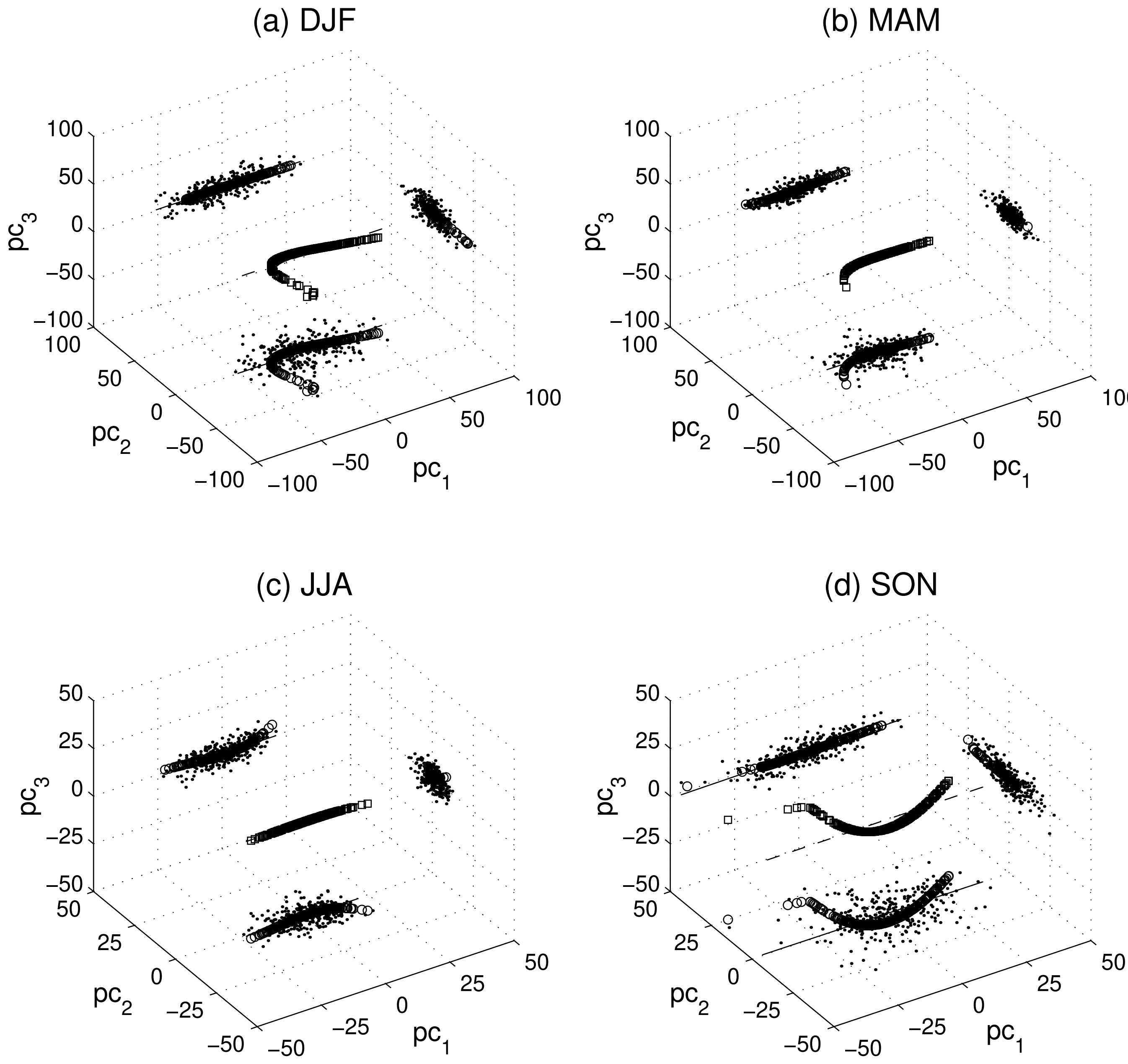

Figure 6: Similar to Fig. 3, but for *S0095*.

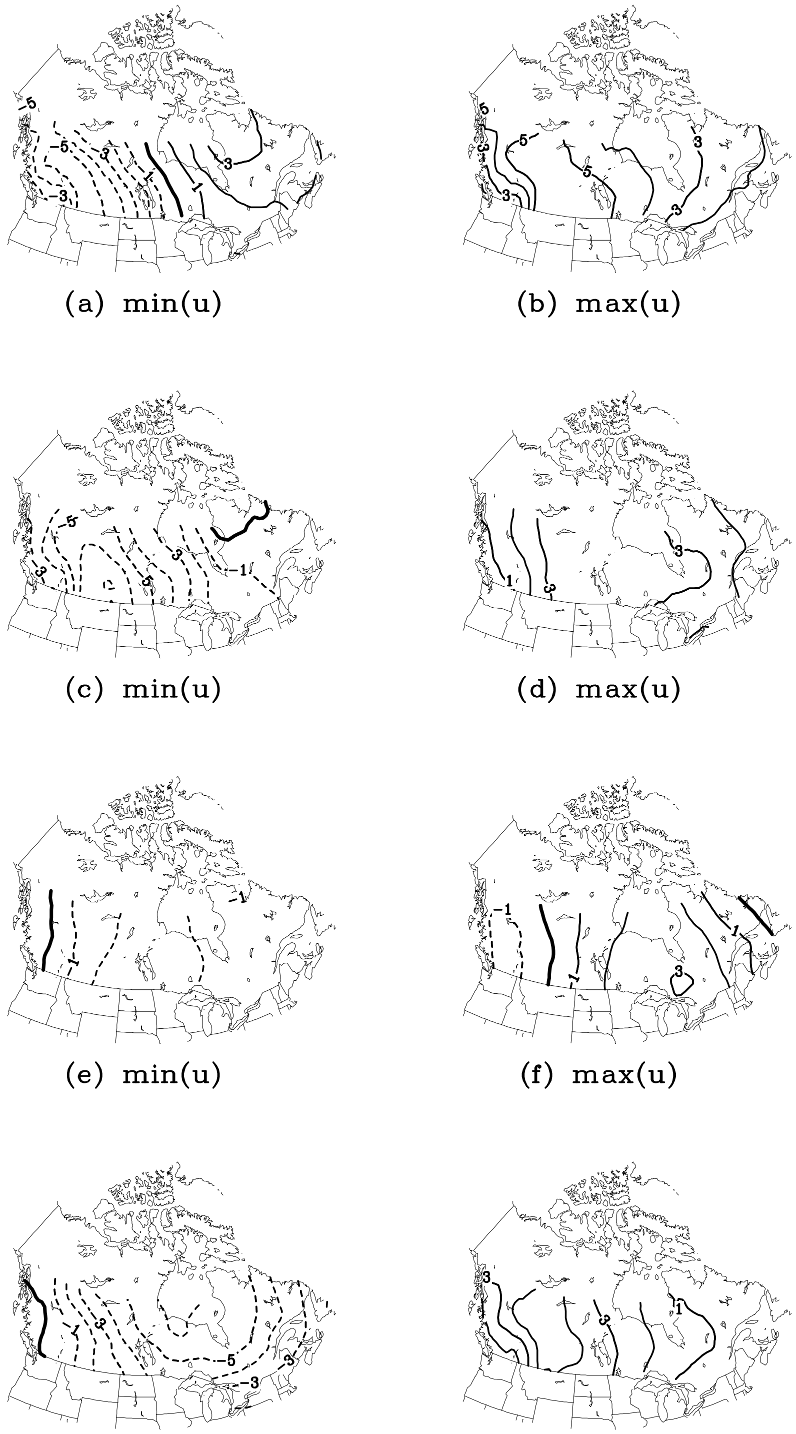

Figure 7: Similar to Fig. 4, but for *S0095*.

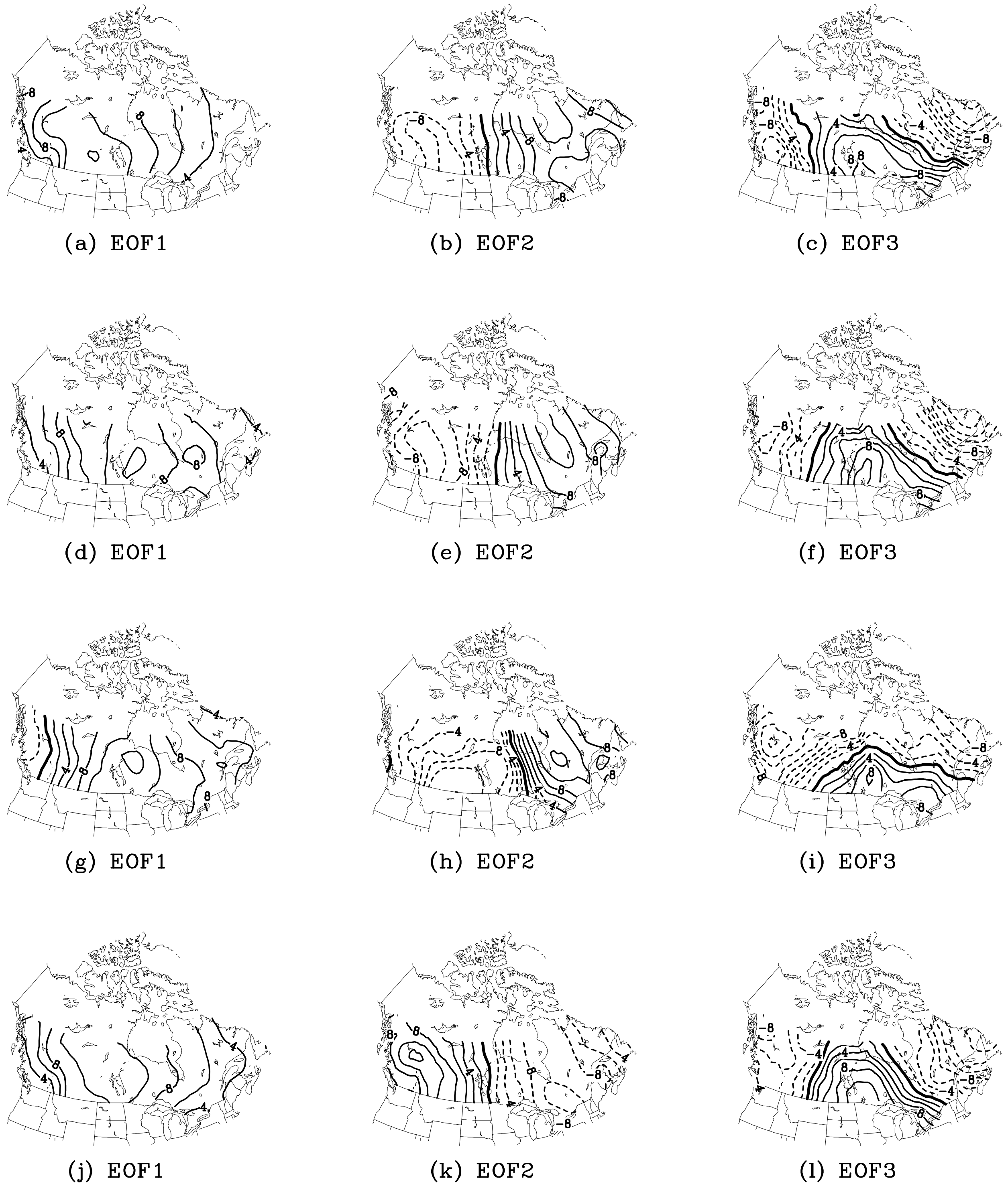

(a) EOF1 (b) EOF2 (c) EOF3

(d) EOF1 (e) EOF2 (f) EOF3

(g) EOF1 (h) EOF2 (i) EOF3

(j) EOF1 (k) EOF2 (l) EOF3

Figure 8: Similar to Fig. 5, but for *S0049*.

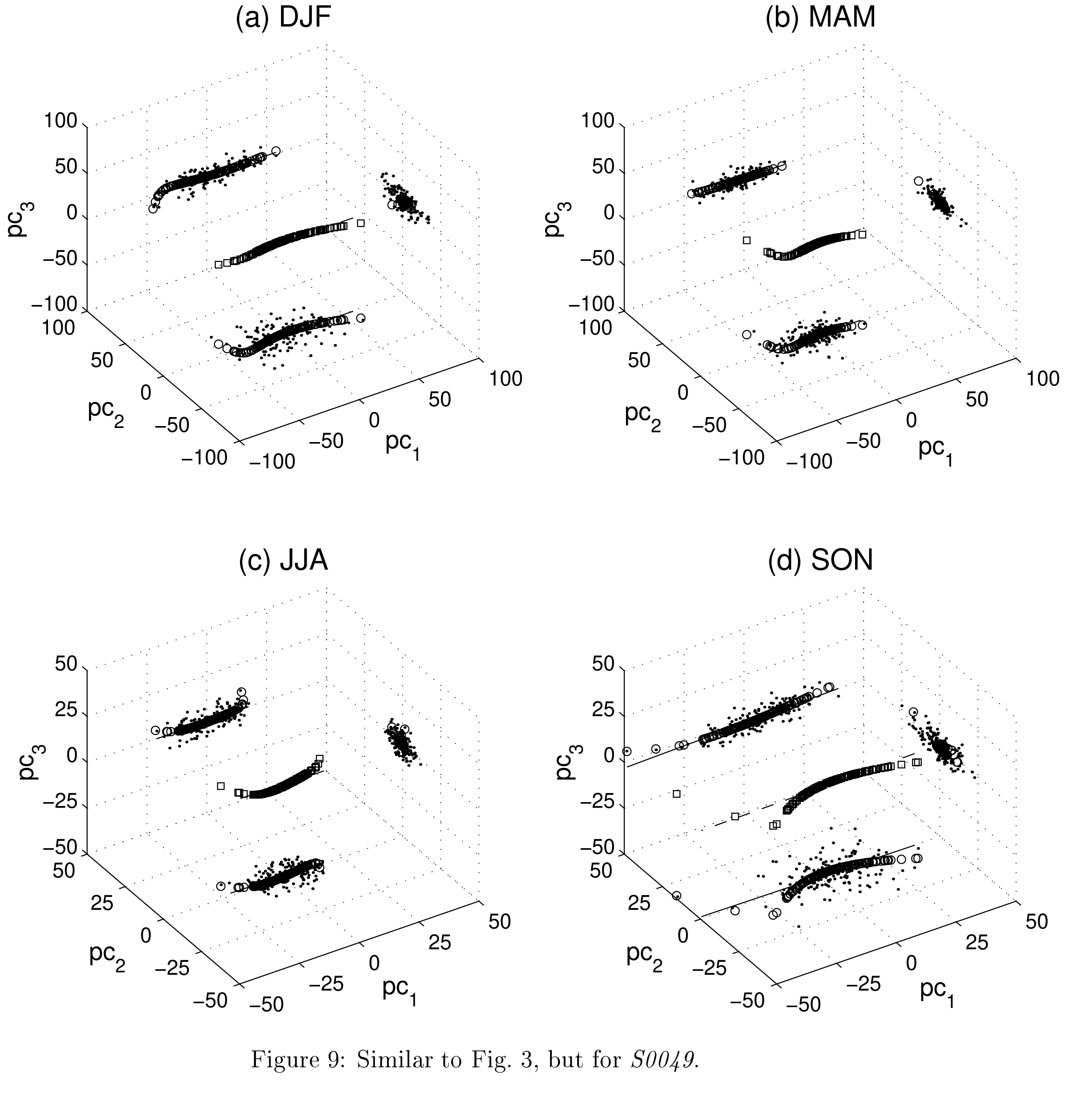

Figure 9: Similar to Fig. 3, but for *S0049*.

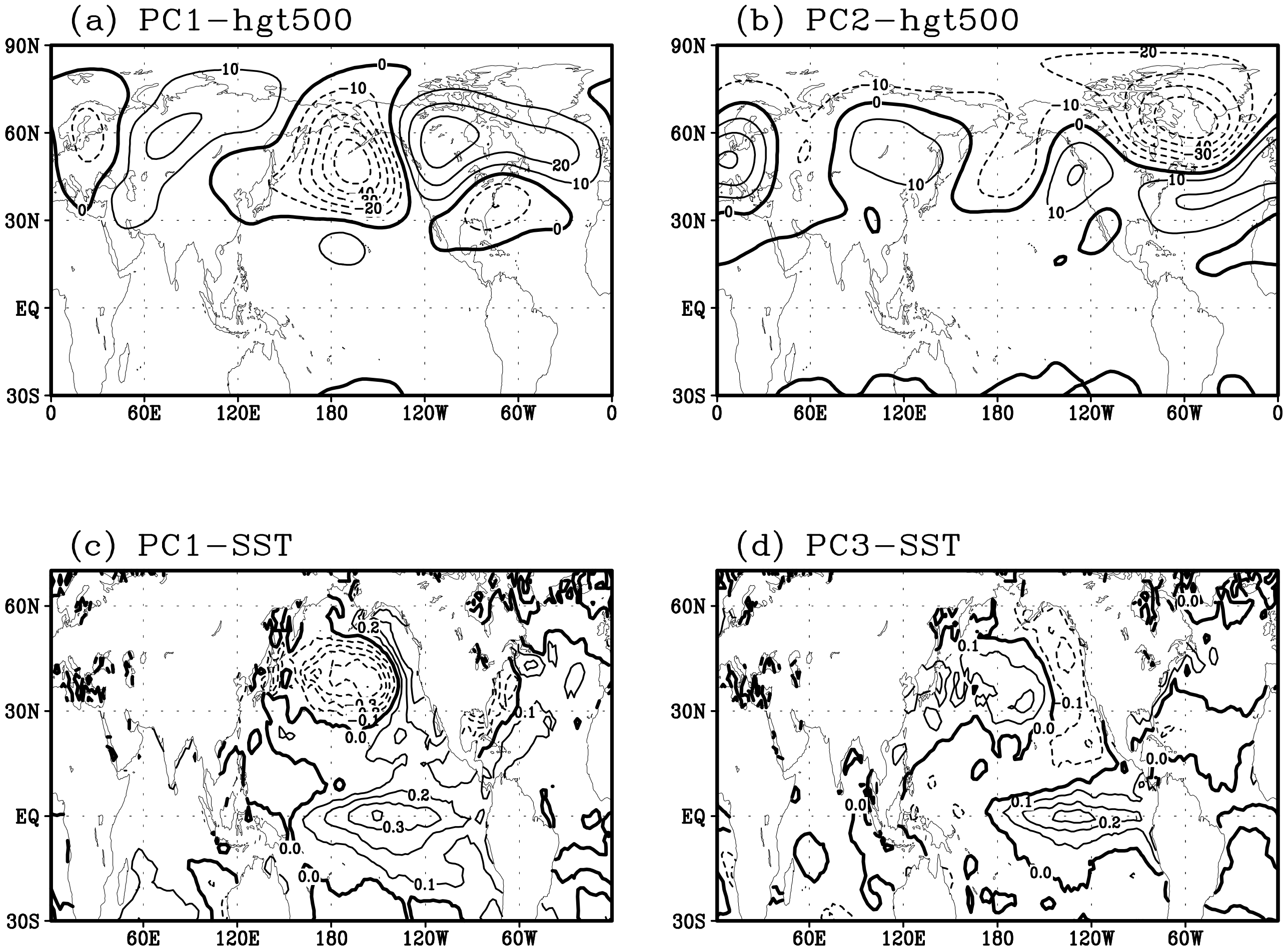

Figure 10: The regression coefficients between the winter 1st PC (of the Canadian SAT anomalies of *C5095*) and the global simultaneous (a) 500-mb height anomalies, and (c) SST anomalies; and the regression coefficients (b) between the winter 2nd PC and the 500-mb height anomalies, and (d) between the winter 3rd PC and the SST anomalies. The regression coefficient shown is the slope, with the PC treated as the independent variable in the regression. Contour interval is 10 in panel (a) and (b), and 0.1 in panel (c) and (d), respectively. The SAT PCs were standardized before performing regression.

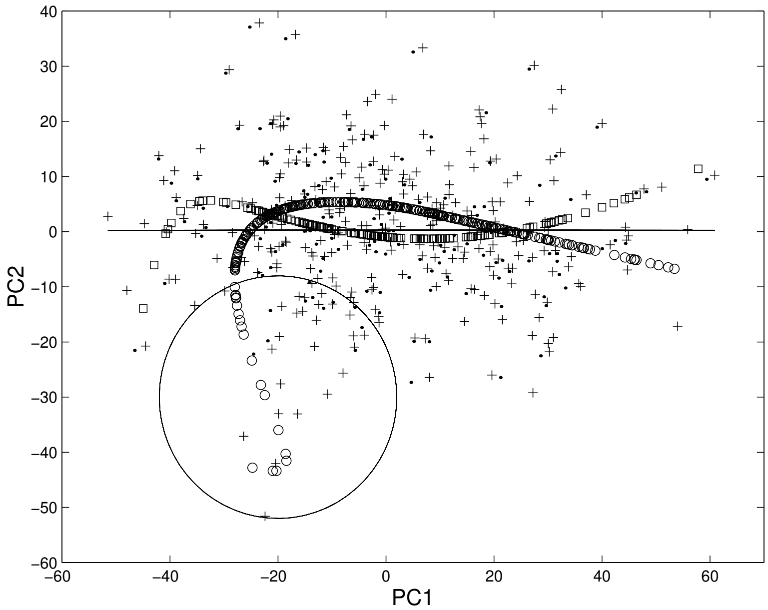

Figure 11: Projections of *S0095* and its leading NLPCA mode onto the PC_1-PC_2 plane, shown by the symbol of plus (+) and overlapping circles. Similarly, projections of *S0049* and its leading NLPCA mode, by scattered dots and overlapping squares, respectively. The big circle includes the data points which possibly contribute to nonlinearity of SAT anomalies after 1950. The straight line represents the PCA mode 1.

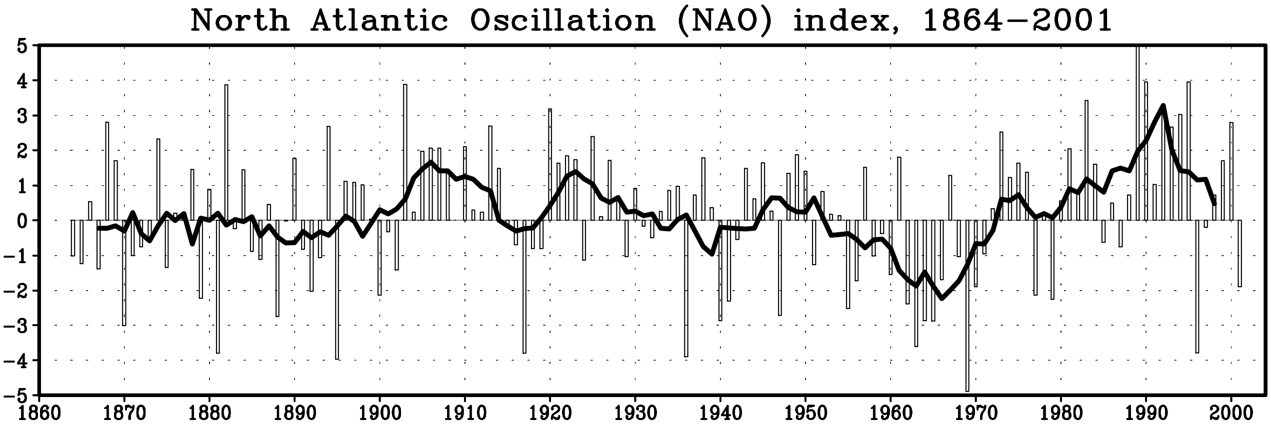

Figure 12: Time series of the winter (December through March) index of the North Atlantic Oscillation (NAO), defined as the difference of normalized sea level pressure (SLP) between Lisbon and Stykkisholmur (Lisbon minus Stykkisholmur) since 1864 to 2001, shown with the hollow bars. A 7-year running mean of the NAO index is displayed by the thick line.